Journal of Materials Chemistry C

Triplet Photodynamic and Up-Conversion Luminescence in Donor-Acceptor Dyads with Slip-stacked vs. Co-facial Arrangement

Journal:	*Journal of Materials Chemistry C*
Manuscript ID	TC-ART-10-2021-005122.R2
Article Type:	Paper
Date Submitted by the Author:	23-Mar-2022
Complete List of Authors:	Yun, Young Ju; University of Illinois at Chicago; Illinois Institute of Technology Peccati, Francesca; Center for Cooperative Research in Biosciences Wiederrecht, Gary P.; Argonne National Laboratory, Center for Nanoscale Materials Gosztola, David; Argonne National Laboratory, Center for Nanoscale Materials Diroll, Benjamin; Argonne National Laboratory, Center for Nanoscale Materials Jiménez-Osés, Gonzalo; CIC bioGUNE, Computational Chemistry Lab Ayitou, A. Jean-Luc; University of Illinois at Chicago, Chemistry; Illinois Institute of Technology, Chemistry

SCHOLARONE™
Manuscripts

Triplet Photodynamic and Up-Conversion Luminescence in Donor-Acceptor Dyads with Slip-stacked vs. Co-facial Arrangement

Young Ju Yun[†,‡], Francesca Peccati[§], Gary P. Wiederrecht[◊], David J. Gosztola[◊], Benjamin T. Diroll[◊], Gonzalo Jiménez-Osés[§,ƒ] and A. Jean-Luc Ayitou*[,†,‡]

[†] *Department of Chemistry, University of Illinois at Chicago, Chicago, IL 60607, United States.*

[‡] *Contribution from the Department of Chemistry, Illinois Institute of Technology, Chicago, IL 60616, United States.*

[§] *Center for Cooperative Research in Biosciences (CIC bioGUNE), Basque Research and Technology Alliance (BRTA), Bizkaia Technology Park, Building 800, 48160 Derio, Spain.*

[ƒ] *Ikerbasque, Basque Foundation for Science, 48013 Bilbao, Spain*

[◊] *Center for Nanoscale Materials, Argonne National Laboratory, Argonne, IL 60439, United States.*

* Corresponding Author e-Mail: aayitou@uic.edu

Abstract: The design/synthesis and characterization of organic donor-acceptor (**D**–**A**) dyads can provide precious data allowing to improve the efficiency of classical photo-induced bimolecular interactions/processes. In this report, two novel triplet **D**–**A** dyads (**4** and **5**) were synthesized and fully characterized. While the optical absorption and emission profiles of these new systems exhibit similar spectral structures as that of the triplet donor/sensitizer quinoidal thioamide (**QDN**), the transient absorption (TA) spectra of these two dyads produced new features that can be associated with triplet transients and charge transfer species. However, the kinetics of the excited-state processes/dynamics is significantly influenced by the geometrical arrangement(s) of donor/acceptor chromophores. Further analysis of the TA data suggests that the dyad with slip-stack geometry (**4**) is less effective in undergoing both intra– and inter–dyad triplet energy transfer than the dyad with co-facial geometry (**5**). Subsequently, triplet sensitization of 9,10-diphenylanthracene (**DPA**) using both dyads led to upconverted photoluminescence via triplet-triplet annihilation of **DPA** triplet transients. But, it was found that a maximum upconversion quantum yield could be achieved at lower power density using the co-facial type dyad **5**. Altogether, these results provide valuable guidance in the design of triplet donor-acceptor dyads, which could be used for light-harvesting/modulation applications.

Keywords: Triplet Energy Transfer; Charge Transfer; Triplet-Triplet Annihilation Photon Upconversion

■ Introduction

Organic triplet donor-acceptor (**D**–**A**) dyads are versatile scaffolds for many light-induced processes *viz.* photovoltaic devices,[1–7] light-emitting diodes,[8–10] and photocatalysis.[11–14] To maximize the efficiency of the aforementioned processes, it is crucial to design/engineer the ideal **D**–**A** scaffolds such that the excited-state interaction(s) between the triplet energy donor (**D)** and the acceptor (**A**) is not constrained by intra-dyad geometrical parameters or extra/inter-dyad quenchers.[15–19] In various pertinent literature, it has been reported that the distance separating the **D**/**A** chromophores,[20] the overlap of the **D**/**A** wavefunctions/orbitals or dipole-dipole interactions,[20,21] the optoelectronic bandgap,[22–24] and the structural orientation of **D**/**A** units can affect the overall photophysics of a triplet dyad.[25–27] For example, Min-Ji *et al.*[25] have found that the geometrical features (*ortho*-, *para*-, and *meta*-) in triplet dyads could impact photophysical events in these systems. Alexei *et al.*[28] also demonstrated that depending on the geometry/length of the molecular linker/spacer in a **D**–**A** dyad, photo-induced energy transfer could follow either the Dexter mechanism or the Forster-type dynamics. The investigation of geometry effect in co-facial type and slip-stacked perylene-diimide (PDI) based dyads (known to undergo singlet fission to generate triplet pairs) have also been investigated by Wasilewski *et al.*[29,30] In this work, it was found that the co-facial type PDI dyad shows the rapid formation of excimer over the slip-stacked system. The investigation of these systems has led to the conclusion that due to slower excitons deactivation, *via excimers formation*, in the slip-stacked **D**–**A** dyad, this scaffold could be used to improve the performance of optoelectronic devices.

Contrary to the investigation by Wasilewski *et al.*, we wish to report two triptycene-based dyads, where the co-facial **D**/**A** interaction(s) is preferred and could lead to efficient intra– and inter-dyad TEnT. The present investigation complements a recent work[22] (from our group), where

a triptycene-based dyad **3** (Fig. 1)–*synthesized from a quinoidal naphthylthioamide (**QDN**) triplet energy donor and 3-ethynyl perylene (**Per**)*–underwent essentially photo-induced charge transfer (CT)[31–34] in place of the desired **QDN→Per** triplet energy flow (TnET) (Supporting Information, Fig. S13).

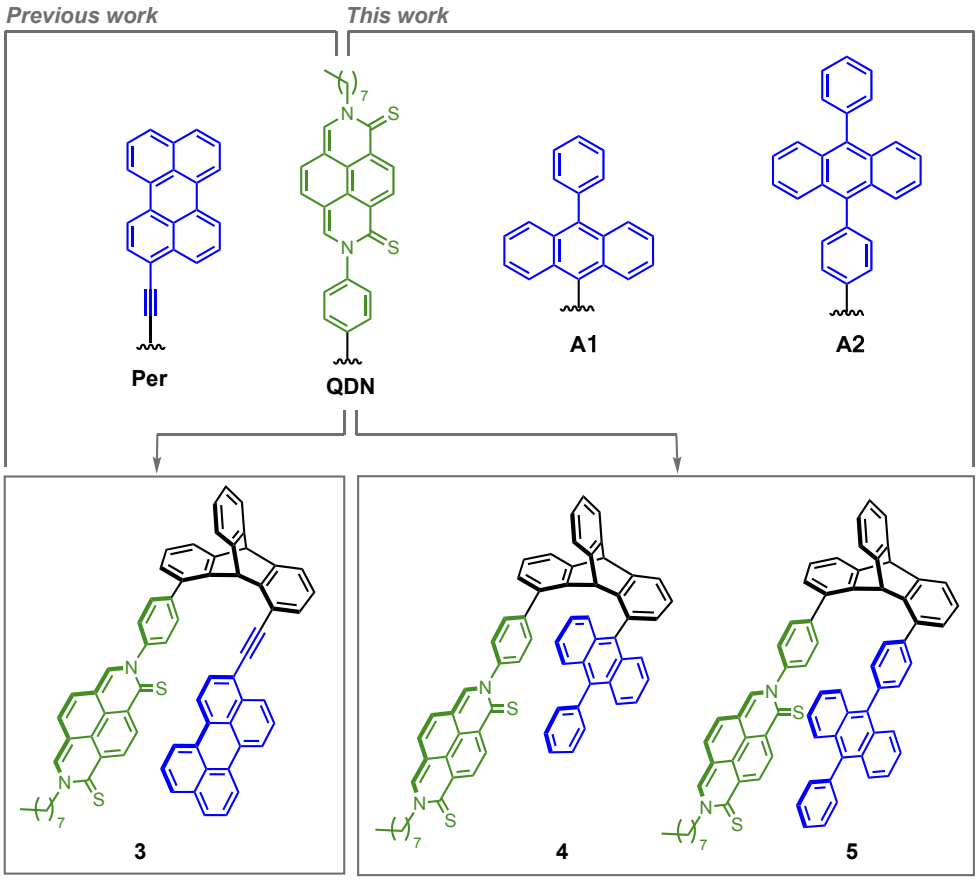

Fig. 1. Chemical structures of the triplet energy donor/sensitizer (**QDN**), acceptors (**Per**, **A1**, and **A2**), and the corresponding dyads **3**, **4**, and **5**.

With dyad **3**, it was further rationalized that the CT dynamics stemmed from a change in the electronic bandgap of the acceptor **Per**. The introduction of the acetylenic spacer has contributed to reducing the HOMO/HOMO-1 levels of the acceptor unit, albeit the triplet energy level of the acceptor ($E_T \approx 1.53$ eV)[35] remains unchanged. Concurrent to the report on dyad **3**, we also

reported[36] that **QDN** (with $E_T \approx 1.77$ eV in DCM at 77 K and 1.67 eV in PEG200) could be used to perform endothermic triplet sensitization of 9,10-diphenyl anthracene (**DPA**) ($E_T \approx 1.78$ eV)[37] leading to **DPA** triplet-triplet annihilation photon upconversion (TTA-UC) with a quantum yield (Φ_{UC}) of 2% (4% after correcting for inner filter effect). By replacing **Per** (in dyad **3**) with **DPA**, it is expected that the **QDN→DPA** TEnT process will not be affected but the issue with mismatched electronic bandgap would be "corrected" based on the relative energies of the frontier molecular orbitals (See Fig. 4). Furthermore, the new molecular dyad(s) exhibits slip-stack and/or co-facial geometrical features, which may influence the kinetics of the **QDN→DPA** TEnT process. Herein, we report the synthesis and photophysical characterization of two triptycene-based dyads **4** and **5** using **anthracene**/**DPA** derivatives **A1** and **A2** (Fig. 1). In the present work, we investigated the kinetics of intra-dyad TEnT as well as intermolecular TEnT in the presence of free **DPA**. While the mechanism of the intermolecular triplet sensitization (via either **QDN** or **A1**/**A2**) cannot be fully elucidated in the present work, spectroscopy tools such as time-resolved pump-probe setup were used to establish that formation of CT species during intra-dyad TEnT could affect the efficiency of the TTA-UC process and/or its underlying photophysical steps.

■ General Methods

The synthetic procedures for all precursors for sensitizer **QDN** and acceptors **A1** & **A2** are reported in the Supporting Information (Schemes S1–S7). All spectroscopy measurements were performed using spectroscopy-grade solvents. All NMR characterizations were carried out on a Bruker 300 MHz spectrometer at 298 K. High-resolution mass spectrum data were recorded on a Bruker microTOF II or Shimadzu IT-TOF spectrometer in positive (ESI+) ion mode. All spectroscopy measurements were performed using spectroscopy-grade solvents. UV-vis

absorption spectra were recorded on an Ocean Optics spectrometer (DH-MINI UV−vis−NIR light source and QE-Pro detector). Emission spectra were recorded on an Edinburgh Instrument FLS980 spectrometer. Time-resolved pump-probe spectroscopy was performed using an amplified Ti:sapphire laser system (Spectra Physics Spitfire) equipped with an optical parametric amplifier (OPA, Light Conversion, TOPAS). This system produces 130 fs pulses at 5 kHz centered at 800 nm. 95% of the output from the amplifier is directed to the OPA to generate tunable pump pulses in the visible and near-infrared spectral regions. For operation with 130 fs temporal resolution, the pump pulse and the remaining 5% of the output from the amplifier are directed to a transient absorption spectrometer (Helios from Ultrafast Systems), where the 5% output is used to generate a continuum probe pulse extending from 450 nm to 1,400 nm by focusing into a thin sapphire window. The pump pulse is chopped at half the repetition rate to measure a difference spectrum for the transient absorption measurement. The incident pump pulse for these experiments at 510 nm had energy on the sample of 300 nJ per pulse, focused to a 200-μm-diameter spot. The transmitted probe light was collected, and fiber optically coupled to a spectrograph that used a visible (Si) array detector. Data were collected for continuum wavelengths from 450 nm to 750 nm as a function of delay track position for the continuum probe relative to the undelayed pump pulse. The temporal chirp of the data was experimentally determined and corrected before analysis. For longer time scale processes, the probe light comes from a continuum light source (EOS from Ultrafast Systems). In this case, the system operates at 1 kHz and has a time resolution of 200ps/point. Decay times of several hundred microseconds can be measured.

Computational Methods: Full geometry optimizations were carried out with Gaussian 16[38] using the CAM-B3LYP hybrid functional[39] and 6-31+G(d,p) basis set[40] with ultrafine integration grids. Bulk solvent effects in dichloromethane and ethanol were considered implicitly through the IEF-

PCM polarizable continuum model.[41] The possibility of different conformations was taken into account for all structures. All stationary points were characterized by a frequency analysis performed at the same level used in the geometry optimizations. Potential energies (ΔE) were used for the discussion on the relative stabilities of the considered structures. The quasiharmonic approximation reported by Truhlar et al. was used to replace the harmonic oscillator approximation for the calculation of the vibrational contribution to enthalpy and entropy.[42] Vertical excitations were computed at the same level of theory with TD-DFT (Tamm-Dancoff approximation[43]) with a linear response non-equilibrium treatment of the solvent.[44] In this regime, only the fast degrees of freedom of the solvent are equilibrated with the excited state electronic redistribution. Computation of solvent accessible surface areas and orbital representation were performed with UCSF Chimera.[45]

TTA-UP Procedure: The upconversion study was performed using a 532 nm continuous wave laser beam (Nd:YAG with varying power from 20 μW to 2500 μW), which was focused onto the samples in a 2 mm cuvette. The laser beam spot size had a diameter of 118 μm. Samples of dyads **4** and **5** were prepared freshly in inhibitor-free THF with 0.1 O.D. at 532 nm, then an equal amount of **DPA** (saturated in THF) was added to each sample followed by 3 cycles of freeze-pump-thaw for deaeration. A 532 band stop filter was used to block the incident light from the detector. Upconverted photoluminescence emissions were collected and processed with Igor Pro v8 software.

■ Syntheses of dyads 4 and 5

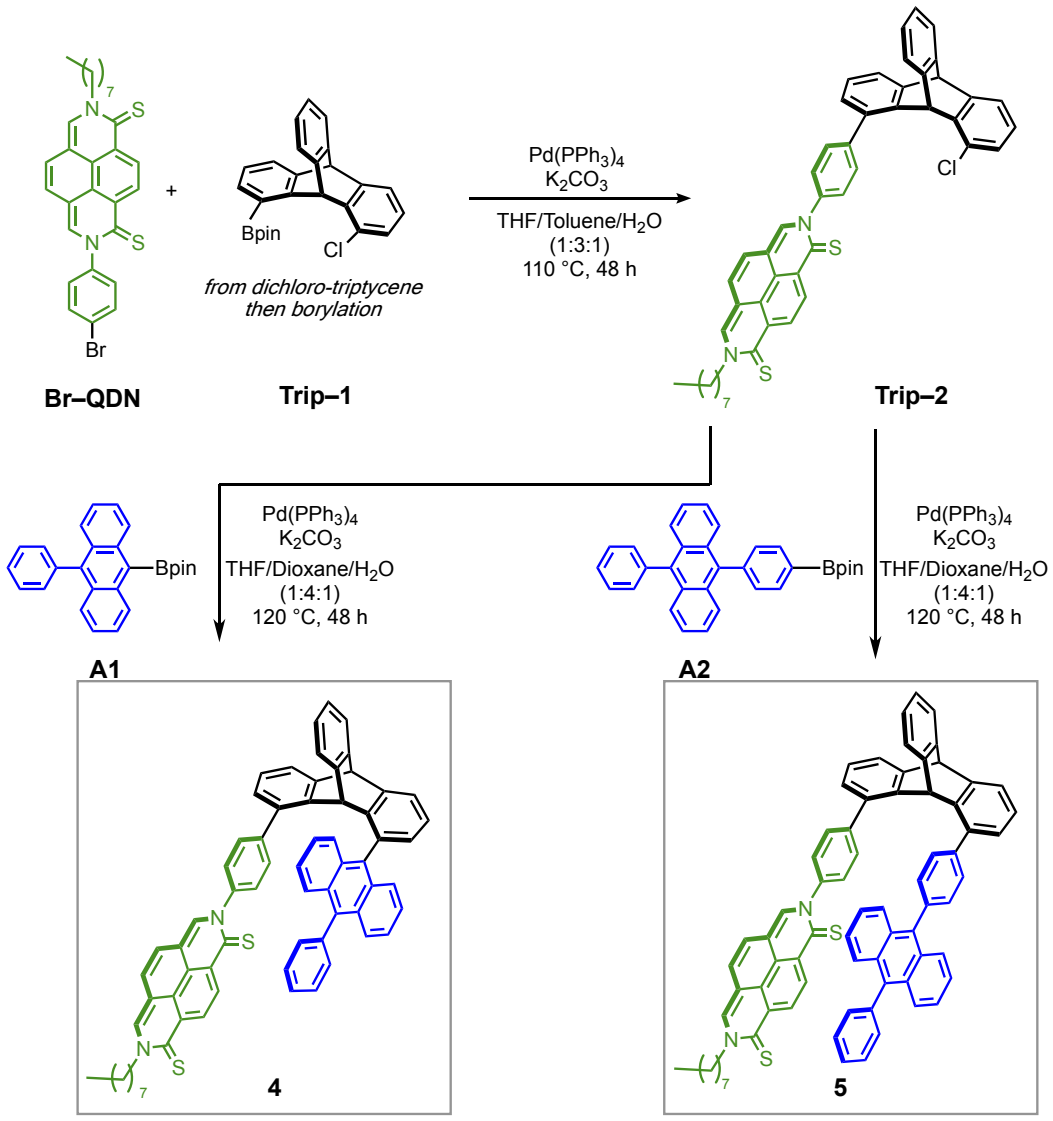

Scheme 1. Syntheses of triptycene-based **D**−**A** dyads **4** and **5**.

Dyad **4** and **5** were synthesized following a convergent synthetic strategy, as shown in Scheme 1. The synthetic procedures for all precursors of dyads **4** and **5** are comprehensively described in the Supporting information (Scheme S1-S7). Triplet sensitizer **QDN (and Br–QDN)** was previously reported by our group.[22,46] Dyad **4** and **5** were synthesized using Suzuki coupling reaction conditions, where **Trip–1** was reacted with **Br–QDN** to afford **Trip–2** (Supporting

Information, Scheme S5). Then, **Trip–2** was reacted with anthracene **A1** or **A2** under Suzuki coupling conditions to afford dyads **4** and **5**, respectively (Supporting Information, Schemes S6, S7). Both **4** and **5** were fully characterized by ^{1}H and ^{13}C NMR (Supporting Information, Fig. S1-S12).

■ Results and Discussion

UV-vis and Emission Spectroscopy

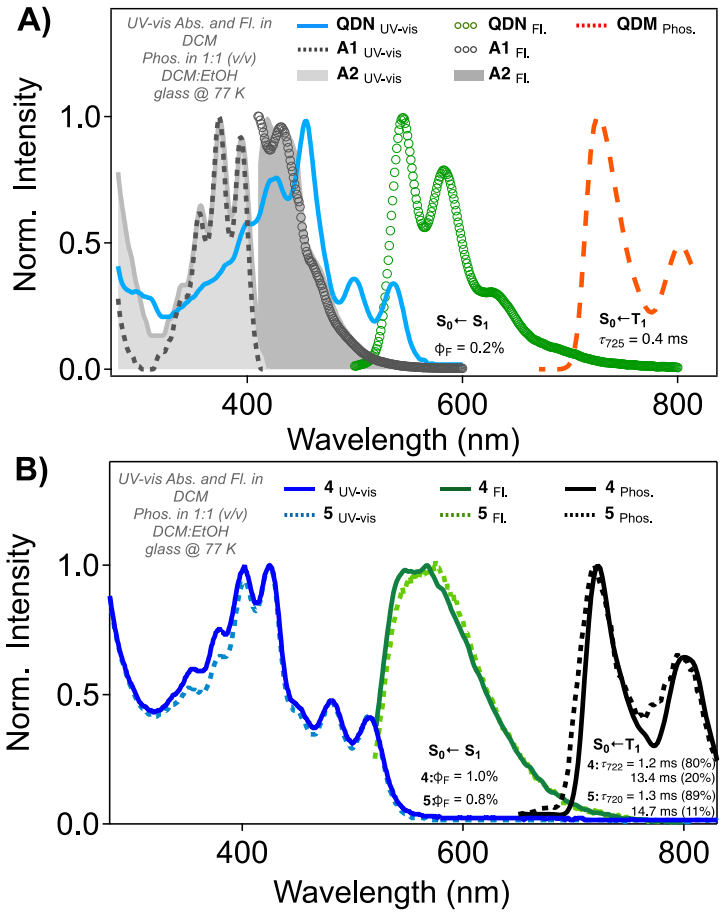

Fig. 2. UV-vis absorption and emission spectra: A) **QDN**, **A1**, and **A2**; B) dyads **4** and **5**. Samples O.D. = 0.2 at λ_{Exc} = 470 nm for **QDN**, O.D. = 0.1 at λ_{Exc} = 400 nm for **A1** and **A2**, and O.D. = 0.1 at λ_{Exc} = 510 nm for **4** and **5**.

Compared to the UV-vis absorption and emission spectra for sensitizer **QDN** and acceptors **A1** & **A2** (Fig. 2A), the spectra of dyads **4** and **5** (Fig. 2B) seemingly exhibit characteristics features from the donor and acceptor(s) chromophores. Similar to parent sensitizer **QDN**, dyads **4** and **5** can also harvest green photons up to ca. 580 nm with noticeable absorption maxima at 402-404 nm. Interestingly, the transition around 450 nm points to an expected ground-state CT species, which has been observed in other investigations from our group.[22] On the photoluminescence behavior(s) of the two dyads, one can see that the fluorescence emission spectra (λ_{exc} = 510 nm) are quite similar, but the band of dyad **5** is slightly red-shifted at ca. 575 nm. For the two dyads, the broad and unstructured fluorescence emission spectra are reminiscent of overlapped transitions from the lowest singlet excited-state and (CT)* species, as observed with dyad **3**.[22] Importantly, the quantum yields (Φ_F) for these emissions (Φ_{F_4} = 0.01 and Φ_{F_5} = 0.008) are four times higher than that of parent sensitizer **QDN** (Φ_{F_QDN} = 0.002) (Table 2) indicating that besides the intrinsic emission from the S_1 of **QDN**, there are additional radiative transitions, presumably from (CT)* species. With these modest Φ_F values from these molecular systems, it was expected that the phosphorescence emission band of the **QDN** chromophore could be recovered (Fig. 2A), unless the $T_1 \leftarrow S_1$ Intersystem Crossing (ISC) is significantly quenched. For both dyads, the phosphorescence emission spectra (recorded at 77 K in ethanol/dichloromethane glassy matrix) exhibit maximum intensities at ca. 722-725 nm (Fig. 2B) with the typical profile of the parent **QDN** chromophore. However, while the phosphorescence decay trace of parent **QDN** was fitted with a mono-exponential function with lifetime τ_{725} = 0.4 ms, the decay traces for both dyads **4** and **5** showed bi-exponential kinetics with lifetimes $\tau_{720/722} \approx$ 1.2 ms (major component) and 14 ms (minor component) (Table 2). Based on our previous investigation with dyad **3**,[22] we

ascertained that the major component (1.2 ms) is the intrinsic phosphorescence lifetime of ^{3}(**QDN**)* unit (within the dyads) and the longer lifetime (14 ms) can be attributed to either the phosphorescence lifetime from ^{3}(**A1**)* /^{3}(**A2**)* or the triplet charge-transfer state ^{3}(CT)* of the dyads.

Conformational Analysis

A conformational analysis of dyads **4** and **5** in the ground state (S_0) was performed in two solvents: dichloromethane and ethanol (Fig. 3) (see Computational Methods). The optimized geometries of four low-energy conformers of each compound and the relative energies are presented in Table 1. No significant difference in the relative conformational energies for each dyad in the two examined solvents was found. Alternative stackings of the donor **QDN** and the **A1**/**A2** moieties yield a variety of conformers in some cases almost degenerate in energy (**4a-c** and **5a-c**).

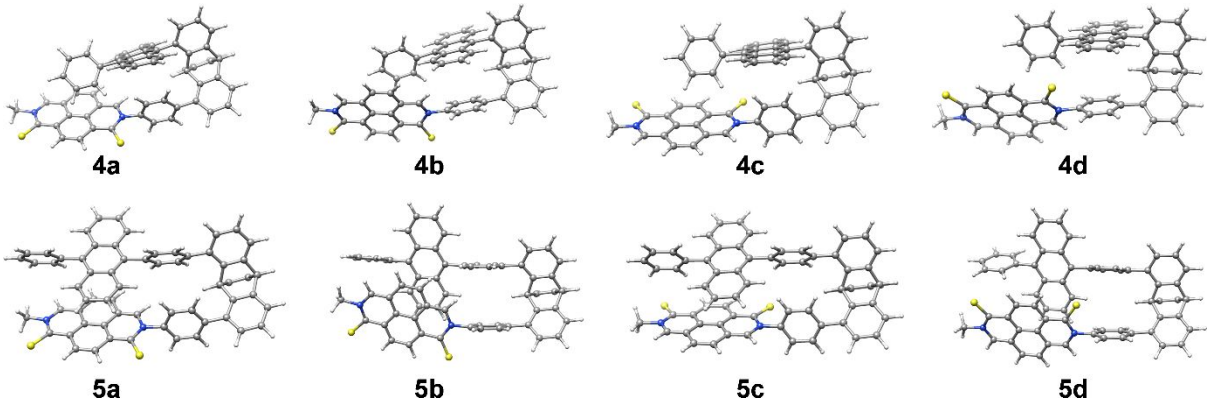

Fig. 3. Geometries of low-energy conformers optimized for **4** and **5** with CAM-B3LYP/6-31+G(d,p) in dichloromethane.

The geometries of both **4** and **5** were re-optimized in the T_1 excited state from their most stable conformers in S_0 (**4a** and **5a**, respectively). In both cases, it was found that the spin density (i.e. the unpaired electrons) was essentially localized on the **QDN** fragment (Fig. 4). Importantly, the calculations also revealed that the energy of the singly occupied molecular orbitals is very similar to that of **4a** and **5a** (data not shown). Vertical excitations to different open-shell singlets calculated through TD-DFT revealed low-wavelength (323-337 nm) charge-transfer (CT) transitions for both dyads **4** and **5** (*see Supporting Information Table S1 and Figures S15–S30*).

Table 1. Relative potential energies (in kcal mol^{-1}) and solvent-accessible surface area (SASA, in A^2) of four low-energy conformers of **4** and **5**. For comparison, the most stable conformer for each compound was arbitrarily assigned zero potential energy.

	$\Delta E_{dichloromethane}$	$\Delta E_{ethanol}$	*SASA*
4a	0.00	0.00	955.36
4b	1.97	1.82	954.10
4c	1.59	1.48	976.56
4d	7.48	7.24	980.41
5a	0.00	0.00	1024.69
5b	0.03	0.04	1024.53
5c	1.52	1.70	1018.11
5d	4.10	4.11	1031.41

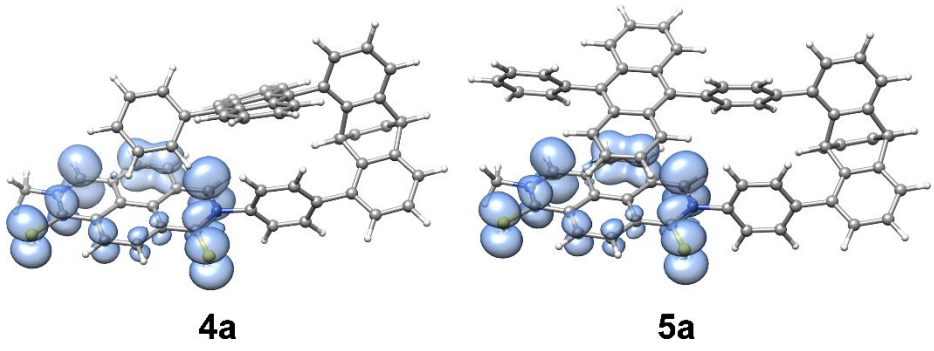

Fig. 4. Spin density at the T_1 optimized geometry of **4a** and **5a** optimized with CAM-B3LYP/6-31+G(d,p) in dichloromethane (surface isovalue = 0.002 a.u.).

Using the solvent-accessible surface area (SASA) method, we established that dyad **5** is more accessible to solvent and other molecules than 4 (Table 1). Hence, we expect that bimolecular $\mathbf{DPA}_{free}\bullet\bullet\bullet\mathbf{DPA}_{dyad}$ interactions would be more efficient in dyad **5** than in **4**.

Transient Absorption Spectroscopy

Next, time-resolved transient absorption spectroscopy (TA) technique was employed to decipher the excited-state dynamics (TEnT or CT) of the dyads upon excitation using pump wavelength 510 nm, where acceptors **A1** and **A2** don't absorb (Fig. 5). As depicted in Fig. 5A,B & 3D,E, the femtosecond TA (ds-TA) spectra of the two dyads show an absorption band between 625 and 720 nm, which was ascribed to the singlet ^{1}(CT)*. Importantly, these absorption bands match the position of the ^{1}(CT)* emission from dyad **3** (Supporting Information, Fig. S13D).[22] However, the absorption signal intensity for the ^{1}(CT)* species is weaker for dyads **4** and **5** than that of **3** (Supporting Information, Fig. S14), which indicates that in addition to the CT process, an efficient ISC is simultaneously occurring through either direct $T_1 \leftarrow S_1$ or triplet CT state. But, the isosbestic point at ca. 630 nm for **4** and 635 nm for **5** indicates an ISC mechanism leading to the formation of the corresponding triplet transients (Fig. 5B and 5E). Analysis of the decay traces of ^{1}(CT)* at 670 nm (**4** and **5**) was fitted with a mono-exponential function with time constants of 34.7 ps for **4** and 43.4 ps for **5**.

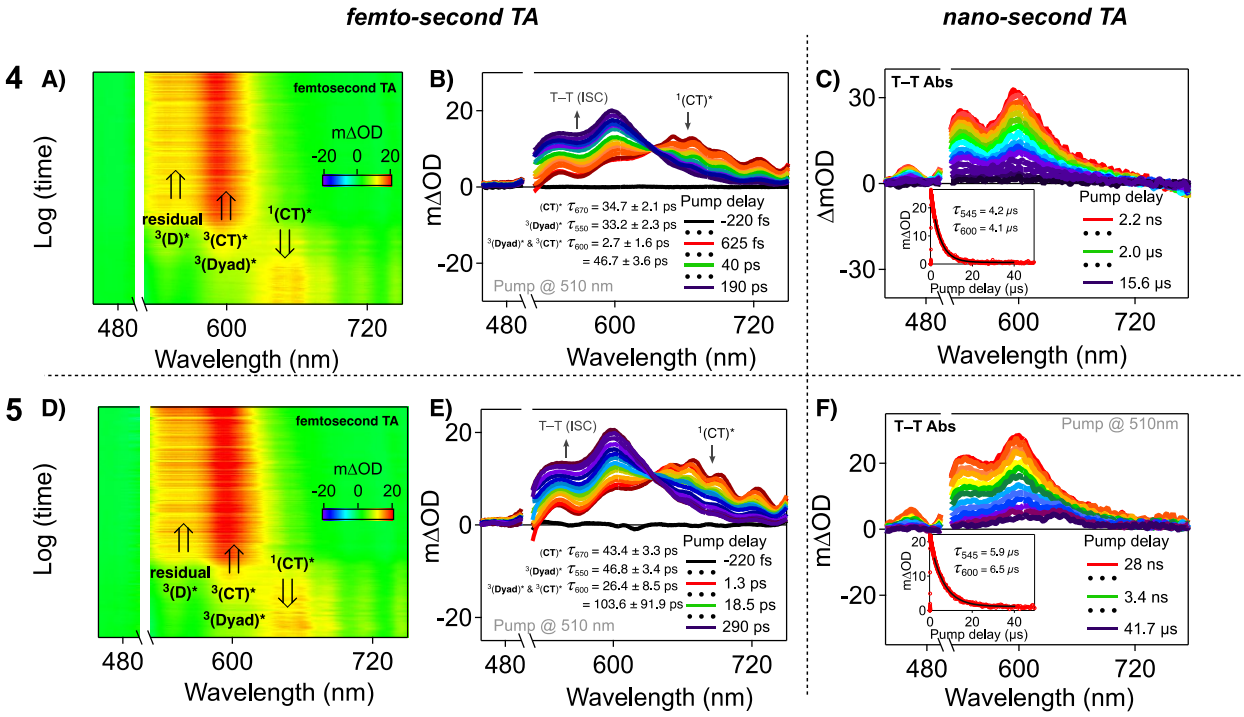

Fig. 5. Time-resolved transient absorption 2D intensity map/spectra for dyads **4** and **5**, and corresponding kinetics recorded in oxygen-free THF samples with optical density O.D. = 0.4 at λ_{Exc} = 510 nm. (A & B) fs-TA map/spectra for **4**; (D & E) fs-TA map/spectra for **5**. (C) ns-TA spectra for **4**; (F) ns-TA spectra for **5**. Pump power = 0.3 μJ/pulse and 2.5 kHz repetition rate for fs-TA and 1 μJ/pulse and 1 kHz repetition rate for ns-TA.

As one can see, the decay of the CT band centered at 670 nm is accompanied by a simultaneous rise of the bands at ca. 600 and 550 nm. While the band centered at 600 nm can be assigned to both ^{3}(CT)* and ^{3}(**4**)*/ ^{3}(**5**)*, the one centered at 550 nm is characteristic of the triplet transients of the **QDN** chromophore. However, for both dyads **4** and **5**, despite that the time constants (33.2 ps for **4** and 46.8 ps for **5**) for the rise of the triplet transient band(s) at 550 nm match well with the decay of the ^{1}(CT)* at 670 nm, these values could also correspond to the time constant for direct $T_1 \leftarrow S_1$ to form the triplet transient of **QDN** (within the dyads). Moreover, using

the bi-exponential function to fit the band centered at 600 nm, it was possible to extra time constants values of (2.7 ps and 46.7 ps) for dyad **4** and (26.4 ps and 103.6 ps) for dyad **5** corresponding to the formation of the ^{3}(CT)* and triplet transients ^{3}(**4**)*/^{3}(**5**)*. From these analyses, it is clear that faster excited-state kinetics observed with the slip-stacked dyad **4** would not be ideal for efficient bimolecular $\mathbf{DPA}_{free}\bullet\bullet\bullet\mathbf{DPA}_{dyad}$ interactions, in agreement with our SASA calculations (Table 1).

Table 2. Optoelectronic data of **QDN**, **4** and **5**.

Entry	*Cpd.*	ε $(M^{-1}cm^{-1})^a$	λ_{Abs}^{max} $(nm)^b$	λ_F^{max} $(nm)^b$	ϕ_F $(\%)^b$	λ_P^{max} $(nm)^e$	τ_P $(ms)^f$	τ_T $(\mu s)^g$
1	**QDN**	12,444	454	545[c]	0.20[c]	725[c]	0.4	10.2[c]
2	**4**	5825.5	402, 404	567[d]	1.00[d]	722[d]	1.2 (80%) 13.4 (20%)	4.2[d]
3	**5**	4191.1	404	575[d]	0.80[d]	720[d]	1.3 (89%) 14.7 (11%)	5.9[d]

[a] Extinction coefficient was measured in THF. [b] UV-vis absorption and fluorescence spectra were recorded in DCM. [c] λ_{Exc} = 470 nm for **QDN** and [d] λ_{Exc} = 510 nm for **4** and **5**. [e] Phosphorescence spectra were measured in 50:50 (v/v) DCM:EtOH glass at 77 K. [f] Phosphorescence decay kinetics. [g] Triplet state lifetime recorded by nanosecond pump-probe method in oxygen-free THF.

If the above analysis holds true, the nanosecond TA (ns-TA) experiments/results will provide additional proofs that geometrical features in the dyads of interest could impact the overall photophysical characteristics including the TTA-UC process. The ns-TA spectra for both dyads show the expected positive absorption bands that correspond to the $T_1 \rightarrow T_n$ (Fig. 5C & 5F), matching the band at a longer time scale in the fs-TA data. The decay traces for these bands at 545 nm was fitted with a mono-exponential function resulting in time constant values of 4.2 μs for **4** and 5.9 μs for **5**. Again, these values are in agreement with the initial hypothesis (*vide supra*) that the slip-stack geometry would induce rapid deactivation of the excited-state of the dyad due to non-ideal orbital interactions (Fig. 6).

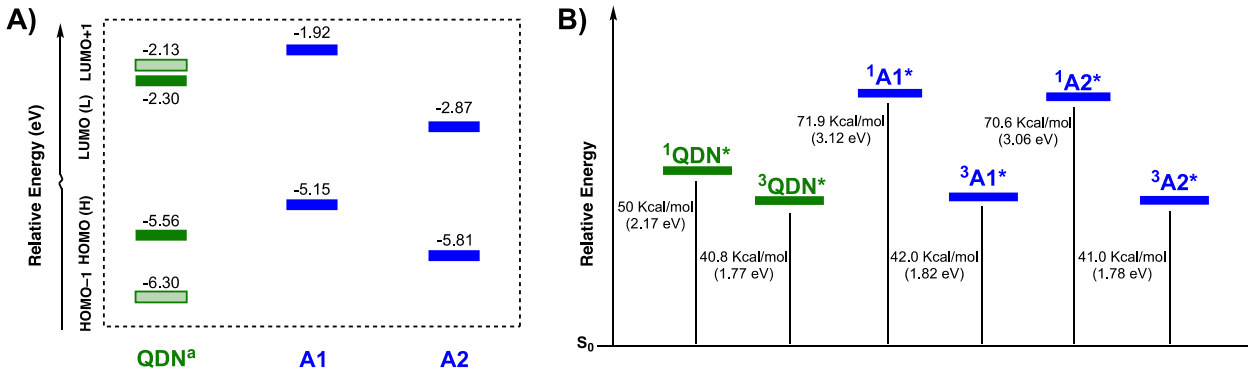

Fig. 6. (A) Optoelectronic bandgap of **QDN** [a], **A1**, and **A2**. (B) singlet/triplet energy levels of **QDN**, **A1**, and **A2**. *Note: **QDN** [a] represents **QDN** with one N-bromo-phenyl substituent.*

From the TA data analyses, we demonstrated that dyads **4** and **5** can still perform both TEnT and CT processes; but the degree of (CT)* formation is significantly reduced in these scaffolds than what was previously observed for dyad **3** (Supporting Information, Fig. S14). In our analysis of the energies of the frontier molecular orbitals and triplet state for the donor and all acceptor units (Fig. 6), we found that while the sensitizer can perform both endothermic and exothermic TEnT to **Per**, **A1**, and **A2**; the HOMO-1 level for **Per** (compared to **A1** and **A2**) is lower in energy than that of the sensitizer **QDN**. Hence, the CT process will be the dominant photophysical process in dyad **3**, whereas in dyads **4** and **5** the TEnT process should be the most favored, but at different degrees.

Compared to dyad **3**, as the dominant process with dyads **4** and **5** is the TEnT, our first instinct was to explore intermolecular (inter-dyad) triplet sensitization of free **DPA** in the solution. With this in mind, the fs-TA and ns-TA experiments were performed using samples of dyad **4**/**5** in the presence of free **DPA** (1:3 molar ratio) so that we can rationales effective DPA/dyad interaction(s) in the excited-state (Fig. 7). In Fig. 7A,B & 7D,E, the TA results show a broadening of the fs-TA

spectra (compared to spectra of the dyads alone). Additionally, these spectra feature different excited-state absorption structures at 670 nm (Fig. 7 & 8), suggesting some interaction between transients of the dyads and **DPA** molecules (**DPA•••D–A** or **D–A•••DPA**). In this scenario, energy transfer to free **DPA** should be expected, and the changes seen in the absorption bands can point to the formation of **DPA** transient(s).

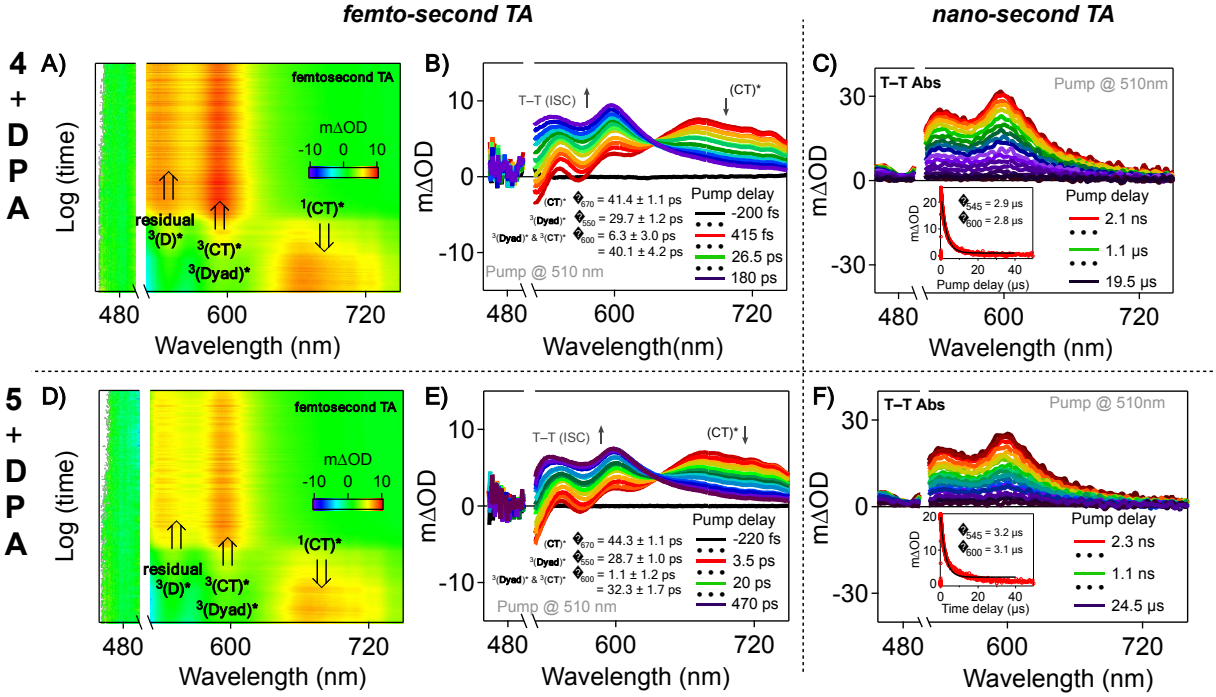

Fig. 7. Time-resolved transient absorption 2D intensity map/spectra for dyads **4** and **5** in the presence of free **DPA** in oxygen-free THF. (A & B) fs-TA map/spectra for **4** + **DPA** and (D &E) fs-TA map/spectra for **5** + **DPA**. Sample O.D. = 0.4 at λ_{Exc} = 510 nm. Pump power = 0.3 µJ/pulse and 2.5 kHz repetition rate for fs-TA and 1 µJ/pulse and 1 kHz repetition rate for ns-TA. *The molar ratio of Dyad:DPA is 1:3.*

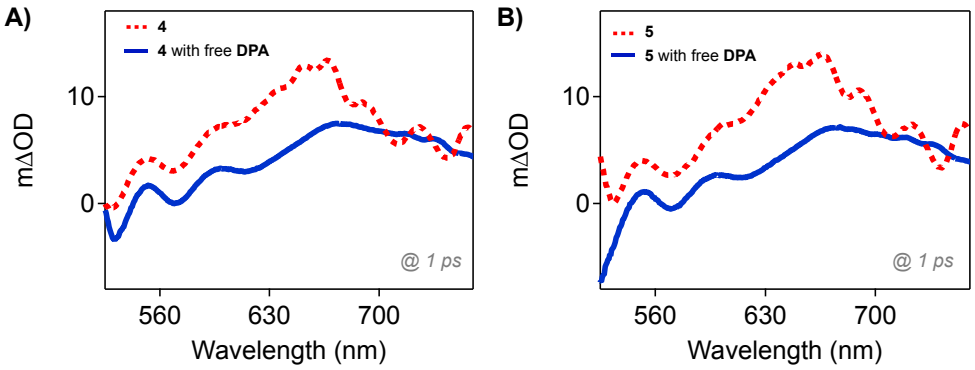

Fig. 8. Differential fs-TA absorption spectra of the dyads (A) **4** and (B) **5** at time 1 ps after pump/pulse: (Red) without free **DPA** and (Blue) in the presence of free **DPA**.

As illustrated in Fig. 8, the comparison of the fs-TA spectra (in the absence and presence of free **DPA**) indicates a decrease in intensity of the absorption band at 640–730 nm, suggesting an inter-dyad TEnT process. Although the direction of the energy transfer could not be established in this work, the analysis of the decay traces for the band centered at 670 nm with free **DPA** produced a longer time constant value (41.4 ps) than the time constant for ^{1}(CT)* from dyad **4** alone (34.7 ps). On the other hand, the kinetic trace of **5** + free **DPA** remained unchanged (ca. 44 ps). The variation in the kinetic of the triplet excited-state for the two samples (Fig. 7C & 7F) suggests that dyad **5** is a better chromophore for intermolecular/inter-dyad TEnT to free **DPA** than dyad **4**. The changes in triplet lifetime went from 4 and 6 μs (for **4** and **5** alone, respectively) to ca. 3 μs for the two dyads indicating that the (**4**)* is dominated by CT dynamics whereas ISC is preferred in dyad **5**, and the later system can perform both intra- and inter-dyad TEnT more efficiently due to its larger, more extended electronic density.

Triplet-Triplet Annihilation Photon Up-Conversion

Samples of dyads **4** and **5** alone did not show any TTA-UC photoluminescence upon excitation at 532 nm. To ascertain the observed inter-dyad TEnT to free **DPA** in solution, we recorded the photoluminescence emission of samples of the dyads + free **DPA** by varying the power density of the 532 nm incident light. The upconverted emission spectrum of **DPA** is shown in Fig. 9A & 9B with λ_{max} = 430; this emission profile matches the intrinsic emission of **DPA** alone (λ_{max} = 400 nm). The residual photoluminescence from the dyads, most likely from the (CT)* state, were also recovered around 540-750 nm. The non-linear/quadratic behavior of the TTA-UC process can be revealed by plotting the corresponding logarithmic values of the emission intensity and the power density (Fig. 9C and 9D). The comprehensive photophysical pathways for the two dyads are described in Fig. 8.

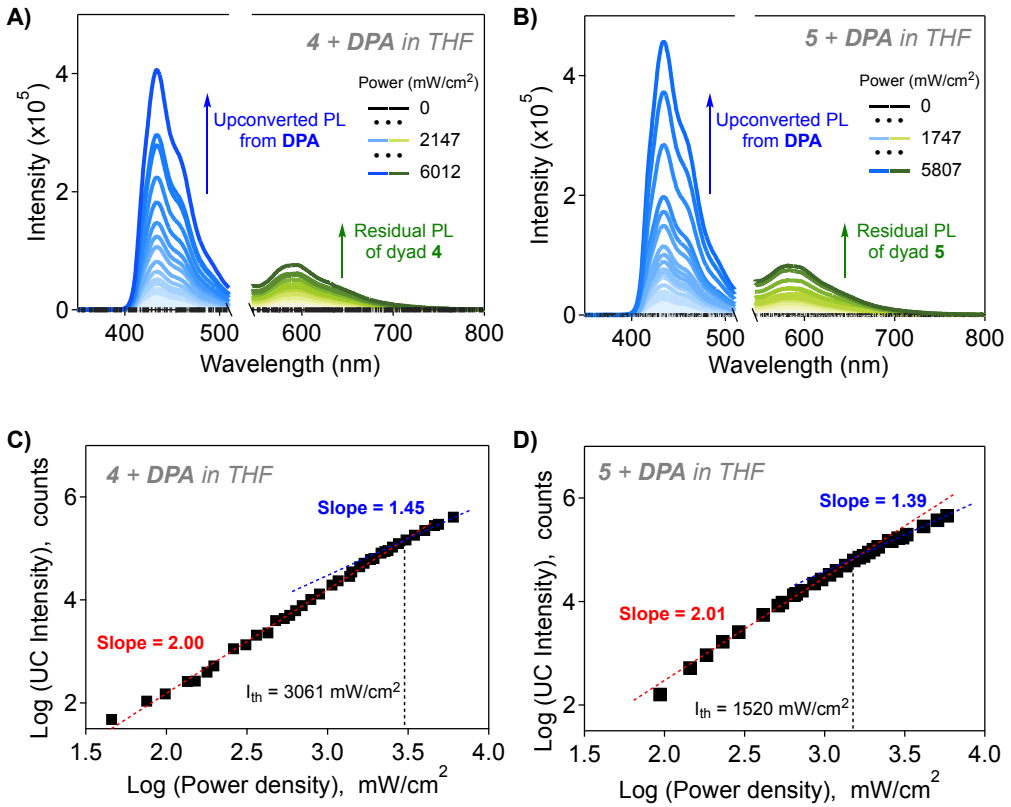

Fig. 9. Upconverted emission spectra of **DPA** in the presence of (A) **4** and (B) **5** excited at 532 nm (samples O.D. = 0.1 at 532 nm) in deaerated THF (3 cycles of freeze-pump-thaw). Double logarithmic plot of the upconverted emission (at λ_{max} = 430 nm) for (C) **4** + **DPA** and (D) **5** + **DPA** as a function of the logarithmic of the power density of the 532 nm Nd:YAG laser.

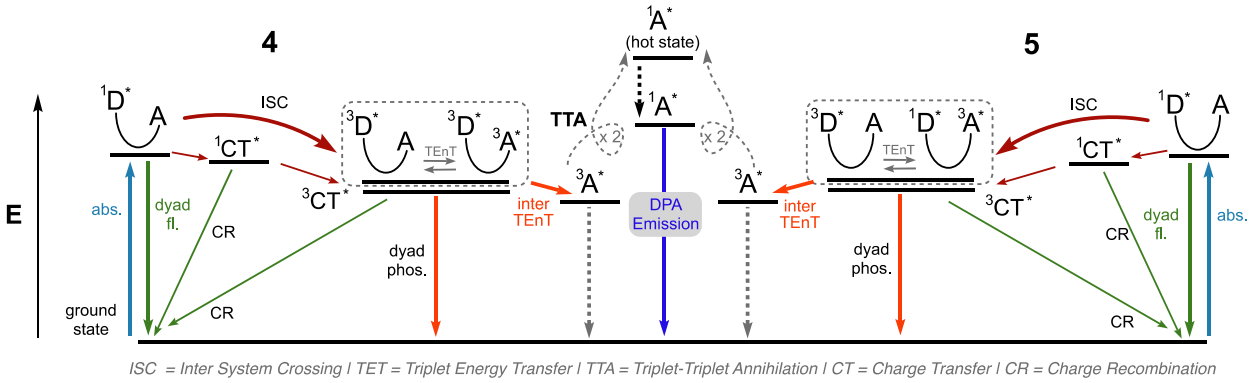

Fig. 10. Photophysical pathway of **4** and **5** (D–A) with TTA-UC process in the existence of free acceptor **DPA** (A).

As one can see, the double logarithmic plots produced slope values of 2.0 and 1.4 for both dyads. The power density threshold (I_{th}), where maximum TTA-UC quantum yield values (Φ_{UC}) will be observed, can be determined by intersecting the low and high power density regimes. The calculated I_{th} for **4** and **5** were 3061 and 1520 mW/cm^2, respectively. The higher value of I_{th} for dyad **4** suggests that the inter-dyad interaction/TEnT with free **DPA** molecules is competing with the formation of the CT state/species. On the other hand, the lower I_{th} value, for co-facial type dyad **5**, correlates with previously reported data (for our group),[36] where the TTA-UC process using free **QDN** and **DPA** chromophores gave Φ_{UC} = 2–4 % in PEG200 with the I_{th} value of 1790 mW/cm^2.

■ Conclusions

Using UV-vis emission and absorption and time-resolved transient spectroscopy tools, we demonstrated that molecular arrangement and interactions in triplet donor-acceptor dyads could influence the overall photophysics *viz.* intra-dyad TEnT and triplet sensitization. Photophysical characterization of dyads **4** and **5** indicated that while impacts resulting from subtle differences in optoelectronic energies between donor **QDN** and the acceptor (**A1** or **A2**) chromophores cannot be ignored, the $T_1 \leftarrow S_1$ ISC was greatly influenced by the donor/acceptor geometrical features. Slip-stacked dyad **4** was found to produce persistent CT species than the co-facial type dyad **5**. On the other hand, the later dyad was found to perform better in terms of intermolecular/inter-dyad TEnT likely due to its larger surface area. Furthermore, dyad **5** can sensitize free **DPA** acceptor at a lower power density than dyad **4 (**1520 vs. 3061 mW/cm^2). Consequently, it was possible to achieve TTA-UC of **DPA** using these dyads as light-harvesting triplet sensitizer(s). The present study provides key/exciting results and a closer step in our ongoing investigation on triplet donor-acceptor dyads, which could be used as single-component chromophores for TTA-UC in the solid state.

SUPPORTING INFORMATION: Details of the synthetic procedures for all precursors of dyads **4** and **5**: ^{1}H and ^{13}C NMR spectra, additional UV-vis absorption spectra, emission spectra, additional computational data. This material is available free of charge via the Internet at http://pubs.rsc.org

AUTHOR INFORMATION:

* A. Jean-Luc Ayitou (**Corresponding Author)**
ORCID: 0000-0001-6355-2564
E-mail: aayitou@uic.edu

Gonzalo Jiménez-Osés
ORCID: 0000-0003-0105-4337

Benjamin T. Diroll
ORCID:

David J. Gosztola
ORCID: 0000-0003-2674-1379

Gary P. Widerrecht
ORCID: 0000-0001-8821-932X

Francesca Peccati
ORCID: 0000-0002-7813-8216

Young Ju Yun
ORCID: 0000-0002-8612-4244

FUNDING SOURCES

National Science Foundation under a CAREER grant no. 1753012 Awarded to AJA.

Illinois Tech Graduate Kilpatrick and Starr Fieldhouse Fellowships to YJY.

Grant RTI2018-099592-B-C22 from the Agencia Estatal Investigacion of Spain (AEI) to G.J.O.

NOTES

The authors declare no competing financial interests.

ACKNOWLEDGMENT:

This material is based upon work supported by the National Science Foundation under a CAREER grant no. 1753012 awarded to AJA. YJY is thankful for the support from the Kilpatrick Graduate Fellowship and the Starr Fieldhouse Research Fellowship Programs at Illinois Tech. GJO thanks the Agencia Estatal Investigacion of Spain for the generous support through the grant RTI2018-099592-B-C22. F. P. thanks the Ministerio de Economía y Competitividad for a Juan de la Cierva Incorporación (IJC2020-045506-I) research contract. Use of the Center for Nanoscale Materials, an Office of Science user facility, was supported by the U.S. Department of Energy, Office of Science, Office of Basic Energy Science, under Contract No. AC02-06CH11357.

■ References

1 R. M. Williams, N. V. Anh and van I. H. M. van Stokkum, *J. Phys. Chem. B*, 2013, **117**, 11239–11248.

2 J. Gong, K. Sumathy, Q. Qiao and Z. Zhou, *Renew. Sust. Energ. Rev*, 2017, **68**, 234–246.

3 V. S. Mothika, P. Sutar, P. Verma, S. Das, S. K. Pati and T. K. Maji, *Chem. Eur. J.*, 2019, **25**, 3867–3874.

4 J. Wang, Z. Chai, S. Liu, M. Fang, K. Chang, M. Han, L. Hong, H. Han and Q. Li, *Chem. Eur. J.*, 2018, **24**, 18032–18042.

5 W. Yang, X. Li, D. Chi, H. Zhang and X. Liu, *Nanotechnology*, 2014, **25**, 482001.

6 T. F. Schulze and T. W. Schmidt, *Energy Environ. Sci.*, 2015, **8**, 103–125.

7 Y. Y. Cheng, A. Nattestad, T. F. Schulze, R. W. MacQueen, B. Fückel, K. Lips, G. G. Wallace, T. Khoury, M. J. Crossley and T. W. Schmidt, *Chem. Sci.*, 2016, **7**, 559–568.

8 A. P. Kulkarni, X. Kong and S. A. Jenekhe, *Adv. Funct. Mater.*, 2006, **16**, 1057–1066.

9 F.-M. Xie, H.Z. Li, G.-L. Dai, Y.-Q. Li, T. Cheng, M. Xie, J.-X. Tang and X. Zhao, *Acs Appl. Mater. Inter*faces., 2019, **11**, 26144–26151.

10 S.-C. Dong, L. Zhang, J. Liang, L.-S. Cui, Q. Li and Z.-Q. Jiang and L.-S. Liao, *J. Phys. Chem. C*, 2014, **118**, 2375–2384.

11 S. Hedström, A. J. Matula and V. S. Batista, *J. Phys. Chem. C*, 2017, **121**, 19053–19062.

12 L. Li, W. Lo, Z. Cai, N. Zhang and L. Yu, *Macromolecules*, 2016, **49**, 6903–6909.

13 A. Hayat, M. U. Rahman, I. Khan, J. Khan, M. Sohail, H. Yasmeen, S. Liu, K. Qi and W. Lv, *Molecules*, 2019, **24**, 1779.

14 S. Haid, M. Marszalek, A. Mishra, M. Wielopolski, J. Teuscher, J.-E. Moser, R. Humphry-Baker, S. M. Zakeeruddin, M. Gratzel and P. Bauerle, *Adv. Funct. Mater.*, 2012, **22**, 1291–1302.

15 D. L. Dexter, *J. Chem. Phys.*, 1953, **21**, 836–850.

16 G. Porter and M. R. Wright, *Discuss. Faraday Soc*, 1959, **27**, 18–27.

17 Y. Zhou, F. N. Castellano, T. W. Schmidt and K. Hanson, *ACS Energy Lett.*, 2020, **5**, 2322–2326.

18 T. N. Singh-Rachford and F. N. Castellano, *Coord. Chem. Rev.*, 2010, **254**, 2560–2573.

19 F. Dumur, N. Gautier, N. Gallego-Plans, Y. Şahin, E. Levillain, N. Mercier, P. Hudhomme, M. Matteo, A. Girlando, V. Lloveras, J. Vidal-Gancedo, J. Veciana and C. Rovira, *J. Org. Chem.*, 2004, **69**, 2164–2177.

20 Y. Zhao, Y. Zhang, X. Lv, Y. Liu, M. Chen, P. Wang, J. Liu and W. Guo, *J. Mater. Chem.*, 2011, **21**, 13168–13171.

21 B. M. Aramburu-Trošelj, I. Ramírez-Wierzbicki, F. Scarcasale, P. S. Oviedo, L. M. Baraldo and A. Cadranel, *J. Phys. Chem. Lett.*, 2020, **11**, 8399–8405.

22 Y. J. Yun, N. Kamatham, M. K. Manna, J. Li, S. Liu, G. P. Wiederrecht, D. J. Gosztola, B. T. Diroll, A. Y. Rogachev and A. J.-L. Ayitou, *J. Phys. Chem. C*, 2020, **124**, 12205–12212.

23 S. Sivalingam, K. Debsharma, A. Dasgupta, S. Sankararaman and E. Prasad, *Chempluschem*, 2019, **84**, 392–402.

24 K.-W. Park, L. A. Serrano, S. Ahn, M. H. Baek, A. A. Wiles, G. Cooke and J. Hong, *Tetrahedron*, 2017, **73**, 1098–1104.

25 M.-J. Kim, M. Ahn, J. H. Shim and K.-R. Wee, *Phys. Chem. Chem. Phys.*, 2020, **22**, 3370–3378.

26 K. Zhou, R. Zhang, J. Liu, M. Li, X. Yu, R. Xing and Y. Han, *Acs Appl. Mater. Interfaces*, 2015, **7**, 25352–25361.

27 Y. Sakata, H. Tsue, M. P. O'Neil, G. P. Wiederrecht and M. R. Wasielewski, *J. Am. Chem. Soc.*, 1994, **116**, 6904–6909.

28 A. Cravcenco, C. Ye, J. Gräfenstein and K. Börjesson, *J. Phys. Chem. A.*, 2020, **124**, 7219–7227.

29 E. A. Margulies, C. E. Miller, Y. Wu, L. Ma, G. C. Schatz, R. M. Young and M. R. Wasielewski, *Nat. Chem.*, 2016, **8**, 1120–1125.

30 E. A. Margulies, L. E. Shoer, S. W. Eaton and M. R. Wasielewski, *Phys. Chem. Chem. Phys.*, 2014, **16**, 23735–23742.

31 M. Kumar, N. Humar, V. Bhalla, H. Singh, P. R. Sharma and T. Kaur, *Org. Lett.*, 2011, **13**, 1422–1425.

32 A. H. A. Clayton, G. D. Scholes, K. P. Ghiggino and M. N. Paddon-Row, *J. Phys. Chem.*, 1996, **100**, 10912–10918.

33 Y.-J. Gong, X.-B. Zhang, C.-C. Zhang, A.-L. Luo, T. Fu, W. Tan, G.-L. Shen and R.-Q. Yu, *Anal. Chem*, 2012, **84**, 10777–10784.

34 J. Morgan, Y. J. Yun and A. J.-L. Ayitou., *Photochem. Photobiol.*, 2022, **98** (**1**), 57–61

35 S. Shokri, G. P. Wiederrecht, D. J. Gosztola and A. J.-L. Ayitou, *J. Phys. Chem. C*, 2017, **121**, 23377–23382.

36 Y. J. Yun, J. Isokuortti, T. Laaksonen, N. Durandin and A. J.-L. Ayitou, *J. Photochem. Photobiol. A*, 2021, **418**, 113412–113418.

37 S. Liu, X. Wang, H. Liu, L. Shen, D. Zhao and X. Li, *J. Mater. Chem. C*, 2020, **8**, 3536–3544.

38 M. J. Frisch, G. W. Trucks, H. B. Schlegel, G. E. Scuseria, M. A. Robb, J. R. Cheeseman, G. Scalmani, V. Barone, G. A. Petersson, H. Nakatsuji, X. Li, M. Caricato, A. V. Marenich, J. Bloino, B. G. Janesko, R. Gomperts, B. Mennucci, H. P. Hratchian, J. V. Ortiz, A. F. Izmaylov, J. L. Sonnenberg, Williams, F. Ding, F. Lipparini, F. Egidi, J. Goings, B. Peng, A. Petrone, T. Henderson, D. Ranasinghe, V. G. Zakrzewski, J. Gao, N. Rega, G. Zheng, W. Liang, M. Hada, M. Ehara, K. Toyota, R. Fukuda, J. Hasegawa, M. Ishida, T. Nakajima, Y. Honda, O. Kitao, H. Nakai, T. Vreven, K. Throssell, J. A. M. Jr, J. E. Peralta, F. Ogliaro, M. J. Bearpark, J. J. Heyd, E. N. Brothers, K. N. Kudin, V. N. Staroverov, T. A. Keith, R. Kobayashi, J. Normand, K. Raghavachari, A. P. Rendell, J. C. Burant, S. S. Iyengar, J. Tomasi, M. Cossi, J. M. Millam, M. Klene, C. Adamo, R. Cammi, J. W. Ochterski, R. L. Martin, K. Morokuma, O. Farkas, J. B. Foresman and D. J. Fox, Gaussian 16 Revision C.01. 2016. 2016.

39 T. Yanai, D. P. Tew and N. C. Handy, *Chem. Phys. Lett.*, 2004, **393**, 51–57.

40 R. Ditchfield, W. J. Hehre and J. A. Pople, *J. Chem. Phys.*, 1971, **54**, 724–728.

41 G. Scalmani and M. J. Frisch, *J. Chem. Phys.*, 2010, **132**, 114110.

42 R. F. Ribeiro, A. V. Marenich, C. J. Cramer and D. G. Truhlar, *J. Phys. Chem. B*, 2011, **115**, 14556–14562.

43 S. Hirata and M. Head-Gordon, *Chem. Phys. Lett.*, 1999, **314**, 291–299.

44 C. Adamo and D. Jacquemin, *Chem. Soc. Rev.*, 2013, **42**, 845–856.

45 E. F. Pettersen, T. D. Goddard, C. C. Huang, G. S. Couch, D. M. Greenblatt, E. C. Meng and T. E. Ferrin, *J. Comput. Chem.*, 2004, **25**, 1605–1612.

46 S. Shokri, J. Li, M. K. Manna, G. P. Wiederrecht, D. J. Gosztola, A. Ugrinov, S. Jockusch, A. Y. Rogachev and A. J.-L. Ayitou, *J. Org. Chem.*, 2017, **82**, 10167–10173.